WATER RESOURCES RESEARCH, VOL. 36, NO. 7, PAGES 1897–1910, JULY 2000

Landslide triggering by rain infiltration

Richard M. Iverson

U.S. Geological Survey, Vancouver, Washington

Abstract. Landsliding in response to rainfall involves physical processes that operate on disparate timescales. Relationships between these timescales guide development of a mathematical model that uses reduced forms of Richards equation to evaluate effects of rainfall infiltration on landslide occurrence, timing, depth, and acceleration in diverse situations. The longest pertinent timescale is A/D_0, where D_0 is the maximum hydraulic diffusivity of the soil and A is the catchment area that potentially affects groundwater pressures at a prospective landslide slip surface location with areal coordinates x, y and depth H. Times greater than A/D_0 are necessary for establishment of steady background water pressures that develop at (x, y, H) in response to rainfall averaged over periods that commonly range from days to many decades. These steady groundwater pressures influence the propensity for landsliding at (x, y, H), but they do not trigger slope failure. Failure results from rainfall over a typically shorter timescale H^2/D_0 associated with transient pore pressure transmission during and following storms. Commonly, this timescale ranges from minutes to months. The shortest timescale affecting landslide responses to rainfall is $\sqrt{H/g}$, where g is the magnitude of gravitational acceleration. Postfailure landslide motion occurs on this timescale, which indicates that the thinnest landslides accelerate most quickly if all other factors are constant. Effects of hydrologic processes on landslide processes across these diverse timescales are encapsulated by a response function, $R(t^*) = \sqrt{t^*/\pi}\,\exp(-1/t^*) - \mathrm{erfc}(1/\sqrt{t^*})$, which depends only on normalized time, t^*. Use of $R(t^*)$ in conjunction with topographic data, rainfall intensity and duration information, an infinite-slope failure criterion, and Newton's second law predicts the timing, depth, and acceleration of rainfall-triggered landslides. Data from contrasting landslides that exhibit rapid, shallow motion and slow, deep-seated motion corroborate these predictions.

1. Introduction

Landslides triggered by rainfall occur in most mountainous landscapes. Some of these landslides occur suddenly and travel many kilometers at high speeds. They can pose grave threats to life and property, as demonstrated in the December 1999 disaster in northern Venezuela [*Larsen et al*., 2000]. Other landslides respond slowly to rainfall and move at imperceptible speeds, but they can dominate sediment yields and landscape change for years or even millennia [*Swanson and Swanston*, 1976]. Traditionally, prediction of rainfall-triggered landslides has relied mostly on recognition of landslide-prone terrain [e.g., *Rib and Liang*, 1978; *Hansen*, 1984; *Soeters and van Westen*, 1996] and identification of rainfall intensities and durations that cause slopes to fail [e.g., *Caine*, 1980; *Cannon and Ellen*, 1985; *Wieczorek*, 1987]. These empirical methods are important, but they provide no theoretical framework for understanding how hydrologic processes influence the location, timing, and rates of landslides or for anticipating how landslide hazards might change in response to changing climate or land use.

Recently, theoretical models have been developed to predict how variations in landslide susceptibility depend on topographic, geologic, and hydrologic variables and changes in land use [e.g., *Sidle*, 1992; *Montgomery and Dietrich*, 1994; *Dietrich et al*., 1995; *Wu and Sidle*, 1995]. All of these models employ the effective stress principle [*Terzaghi*, 1925] in an infinite-slope stability analysis [*Haefeli*, 1948; *Taylor*, 1948], which relates landslide potential to groundwater pressures in discrete landscape cells. The models assume that rainfall influences groundwater only by modulating steady or quasi-steady water table heights and that groundwater flows exclusively parallel to the slope. The models consequently neglect slope-normal redistribution of groundwater pressures associated with transient infiltration of rain. This neglect is predicated more on expedience than physical evidence; both theory and measurements indicate that groundwater pressures in hillslopes respond strongly to transient rainfall and that pressure redistribution includes a large component normal to the slope [e.g., *Freeze*, 1974; *Iverson and Major*, 1987; *Reid et al*., 1988; *Haneberg*, 1991; *Baum and Reid*, 1995; *Iverson et al*., 1997; *Torres et al*., 1998].

To assess the effects of transient rainfall on timing, rates, and locations of landslides, I use rational approximations to develop a theoretical model that augments steady and quasi-steady models such as those described above. Analysis of *Richards* [1931] equation yields approximations that describe near-surface groundwater pressures that develop in hillslopes in response to rainfall over varying periods of time. An approximation valid for long times governs quasi-steady background pressures that typically develop over periods ranging from days to many decades. These pressures reflect the influence of topography, geology, and climate on slope failure potential. An approximation valid for shorter times governs groundwater pressures that develop in response to individual rainstorms or groups of storms and that trigger most dangerous landslides. For slopes that are initially quite wet, the short-time approxi-

Paper number 2000WR900090.

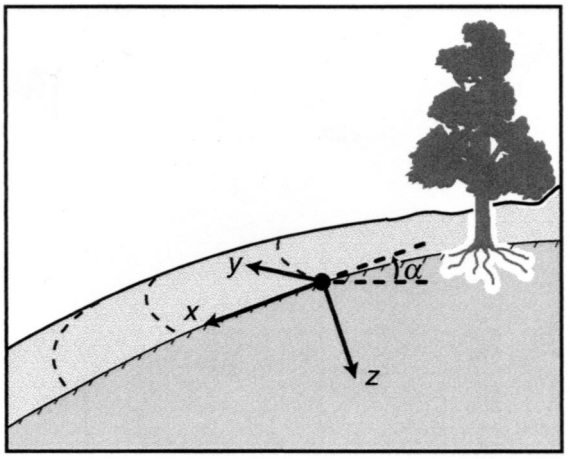

Figure 1. Definition of the local, rectangular, Cartesian coordinate system used to analyze Richards equation. The origin lies on the ground surface, x is tangent to the local surface slope, y is tangent to the local topographic contour, and z is normal to the x-y plane. The slope angle α is measured with respect to horizontal.

mation reduces to a linear diffusion equation, and analytical solutions predict how near-surface pore water pressures respond to rainfall of arbitrary intensity and duration. Combination of a diffusion solution with a generalized infinite-slope stability model and Newton's second law yields an equation that predicts the timing, depth, and rate of slope failure as a function of rainfall intensity and duration. Comparisons of these predictions with data from two well-documented cases demonstrates the utility of the model.

Before detailing the analyses outlined above, it is perhaps worthwhile to emphasize that the theory is born of compromise. The theory aims to predict variations in landslide susceptibility and behavior under diverse geologic and hydrologic conditions, with the caveat that only valid approximations and minimal data inputs are desirable. A more precise theory would avoid approximations and include all details of transient, variably saturated groundwater flow as well as three-dimensional landslide geometries and geologic heterogeneities but would also demand extraordinary data inputs. Conversely, theories that disregard transient rainfall entirely cannot account for its effect on landsliding: an effect that is evident to even casual observers. The new theory described here includes transient rainfall effects but requires only meager data inputs (rainfall intensity and duration and a characteristic hydraulic diffusivity) in addition to those required by steady and quasi-steady theories. A theory this simple cannot, of course, predict all complexities observed in the field. Nonetheless, it can illuminate rainfall effects on the timing and style of landsliding, and it can sharpen the focus of field investigations and model prognostications.

2. Analysis of Hydrologic Processes

To assess the influence of rainfall on near-surface groundwater pressures in slopes, consider a local rectangular Cartesian coordinate system with its origin at an arbitrary point on the ground surface (Figure 1). The coordinate x points down the slope, y points tangent to the topographic contour that passes through the origin, and z points into the slope, normal to the x-y plane. Richards equation governs unsteady, variably saturated, Darcian flow of groundwater in response to rainfall on the slope. Referenced to the coordinate system of Figure 1, Richards equation may be written as [*Bear*, 1972; *Hurley and Pantelis*, 1985]

$$\frac{\partial \psi}{\partial t}\frac{d\theta}{d\psi} = \frac{\partial}{\partial x}\left[K_L(\psi)\left(\frac{\partial \psi}{\partial x} - \sin\alpha\right)\right] + \frac{\partial}{\partial y}\left[K_L(\psi)\left(\frac{\partial \psi}{\partial y}\right)\right] + \frac{\partial}{\partial z}\left[K_z(\psi)\left(\frac{\partial \psi}{\partial z} - \cos\alpha\right)\right], \quad (1)$$

in which ψ is groundwater pressure head, θ is soil volumetric water content, t is time, and α is the slope angle, $0 \le \alpha < 90°$. Terms can be added to (1) to make the x and y coordinates conform with hillslope curvature, but such terms are generally small and vanish in approximations that are valid at shallow depths [e.g., *Hurley and Pantelis*, 1985]. Non-Darcian flow in slopes is not represented by (1) but might be simulated satisfactorily by assigning Darcian parameter values that mimic non-Darcian properties.

The key Darcian parameters in (1) are the hydraulic conductivities in the lateral (x and y) directions and slope-normal (z) direction, K_L and K_z. The conductivities may vary owing to variations of soil properties or ψ. It is convenient to define normalized conductivities K^* with reference to the maximum (saturated) conductivity anywhere within the flow domain, K_{sat},

$$K_L^* = \frac{K_L(\psi)}{K_{\text{sat}}},\ K_z^* = \frac{K_z(\psi)}{K_{\text{sat}}} \quad (2)$$

and to relate the conductivities to hydraulic diffusivities (D_L, D_z, D_0) by

$$D_L = \frac{K_L(\psi)}{C(\psi)},\ D_z = \frac{K_z(\psi)}{C(\psi)},\ D_0 = \frac{K_{\text{sat}}}{C_0}, \quad (3)$$

where $C(\psi) = d\theta/d\psi$ is the change in volumetric water content per unit change in pressure head and C_0 is the minimum value of $C(\psi)$, typically observed when the soil becomes saturated. Thus D_0 is the maximum characteristic diffusivity governing transmission of pressure head, and it thereby provides a convenient reference diffusivity.

Normalization of (1) reveals some fundamental features of hillslope responses to rainfall [*Hurley and Pantelis*, 1985; *Haneberg*, 1991]. In the present context the goal of normalization is assessment of the pore pressure response at depth $z = H$ (measured normal to the slope) and areal position (x, y) as a function of time (Figures 1 and 2). Areal position determines the extent to which rain infiltration elsewhere in the catchment affects the pressure head at (x, y, H). Therefore I define normalized variables

$$\psi^* = \frac{\psi}{H},\ z^* = \frac{z}{H},\ x^* = \frac{x}{\sqrt{A}},\ y^* = \frac{y}{\sqrt{A}} \quad (4)$$

that involve two length scales. One scale is H, which applies in the z direction and establishes an appropriate reference for the pressure head ψ that develops at depth H in response to rainfall. The length scale in the x and y directions is $\sqrt{A}$, where A is the catchment area that might ultimately influence $\psi(x, y, H, t)$ if rainfall persists. Groundwater hydraulics dictates that A may be somewhat ambiguous, because groundwater can cross beneath topographic divides and influence pressures upstream as well as downstream within a flow field. To define an

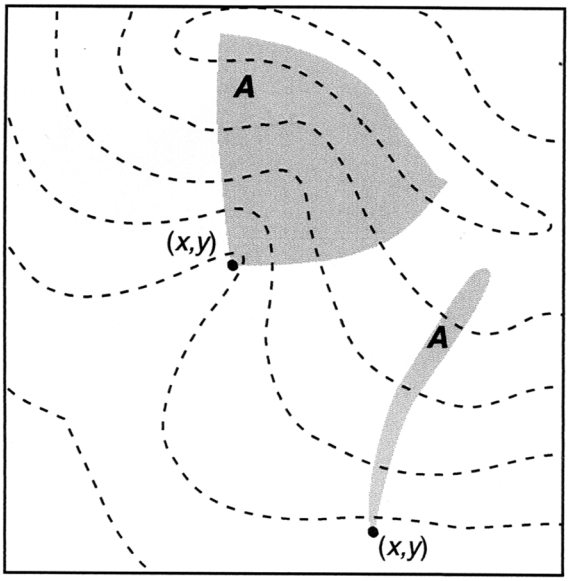

Figure 2. Definition of the planimetric contributing area A at two locations (x, y) in a hypothetical landscape. Dashed lines represent topographic contours.

unambiguous length scale, it is therefore necessary to approximate A by some readily measurable property.

To establish connections with previous work [e.g., *Montgomery and Dietrich*, 1994; *Dietrich et al*., 1995], I approximate A by the area enclosed by the upslope topographic divide and hypothetical flow lines that run normal to topographic contours and bound the region that can contribute surface runoff to point (x, y) (Figure 2). Unless groundwater flow paths are unusually aberrant, this definition of A establishes a length scale $\sqrt{A}$ of the correct magnitude for lateral transmission of pore water pressure to (x, y, H).

Pore pressure transmission in response to rainfall is a transient process, which implies that two timescales exist in conjunction with the two length scales H and $\sqrt{A}$. Employing the reference diffusivity D_0 to establish a reference time, one timescale may be identified as A/D_0, which approximates the minimum time necessary for strong lateral pore pressure transmission from the area A to the point (x, y, H). The other timescale is H^2/D_0, which approximates the minimum time necessary for strong slope-normal pore pressure transmission from the ground surface to depth H [cf. *Iverson and Major*, 1987; *Haneberg*, 1991; *Reid*, 1994]. Here the distinction between pore pressure transmission and water flux is relevant. Rainwater can infiltrate the soil as a gravity-driven slug with uniform water content and zero pore water pressure behind the wetting front [*Bear*, 1972, chapter 9], but pore pressure change in a porous medium is largely a diffusive process that can occur with or without much water flux [cf. *Biot*, 1941, 1956; *Chandler and Johnson*, 1981].

The ratio of the pressure diffusion timescales H^2/D_0 and A/D_0 yields a length scale ratio ε that plays a key role in analyzing pressure head responses to rainfall on slopes,

$$\varepsilon = \sqrt{\frac{H^2 D_0}{A D_0}} = \frac{H}{\sqrt{A}}. \tag{5}$$

If $\varepsilon \ll 1$, long-term and short-term pressure head responses at locations (x, y, H) may be described adequately by simplified forms of Richards equation. In many landscapes with high potential for landslides, values $\varepsilon \leq 0.1$ apply at typical slip surface depths and locations (Table 1). Simplified forms of Richards equation therefore provide a rational basis for assessing landslide responses to rainfall.

2.1. Long-Term Behavior

Long-term pressure head responses can be assessed by identifying the appropriate dimensionless time as $t^* = tD_0/A$ and substituting this expression together with (2), (3), and (4) into (1). Then multiplication of all terms by H/K_{sat} and some algebraic simplification yields a form of Richards equation appropriately scaled to assess $\psi(x, y, H, t)$ in response to rainfall of long duration $(t > A/D_0)$

$$\varepsilon^2 \frac{C(\psi)}{C_0} \frac{\partial \psi^*}{\partial t^*} = \varepsilon^2 \frac{\partial}{\partial x^*}\left[K_L^*\left(\frac{\partial \psi^*}{\partial x^*} - \frac{1}{\varepsilon} \sin \alpha \right) \right] + \varepsilon^2 \frac{\partial}{\partial y^*}\left[K_L^*\left(\frac{\partial \psi^*}{\partial y^*} \right) \right] + \frac{\partial}{\partial z^*}\left[K_z^*\left(\frac{\partial \psi^*}{\partial z^*} - \cos \alpha \right) \right]. \tag{6}$$

Table 1. Characteristic Timescales and Timescale Ratios for Contrasting Landslide Sites

	Significance	Numerical Values	
		Case 1 (Coos Bay)	Case 2 (Minor Creek)
Timescale			
A/D_0	quasi-steady groundwater response time	1 day	300 years
H^2/D_0	transient groundwater response time	20 min	1 year
$\sqrt{H/g}$	landslide acceleration time	0.3 s	0.8 s
T	rainfall duration (example)	1 hour	4 months
Timescale ratios			
ε	$=H/\sqrt{A}$	0.1	0.06
T^*	$\sim T/(H^2/4D_0)$	10	1
S	$\sim (H^2/4D_0)/\sqrt{H/g}$	800	1×10^7

Case 1 is similar to the Coos Bay, Oregon, site described by *Montgomery et al*. [1997] and *Torres et al*. [1998] and assumes $H \sim 1$ m, $A \sim 100$ m^2, and $D_0 \sim 10^{-3}$ m^2/s. Case 2 is similar to the Minor Creek, California, site described by *Iverson* [1984, 1986] and *Iverson and Major* [1987] and assumes $H \sim 6$ m, $A \sim 10^4$ m^2, and $D_0 \sim 10^{-6}$ m^2/s. In each case, timescales are evaluated for a typical point near the failure surface, and for convenience it is assumed that $H = Z$ and $\hat{D} = 4D_0$. Numerical values are rounded to one significant digit.

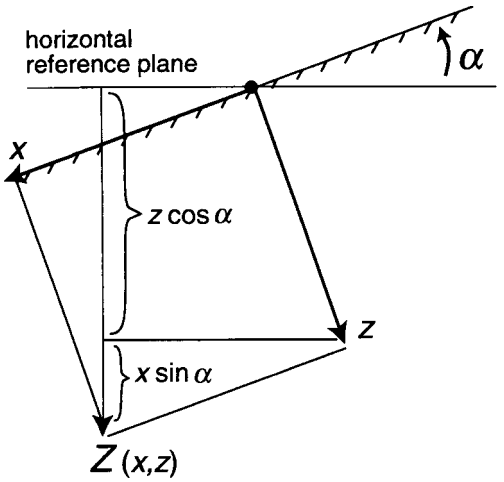

Figure 3. Definition of the vertical coordinate $Z = x \sin \alpha + z \cos \alpha$ used to calculate elevation head or depth at an arbitrary location (x, y). If the Z and z coordinates share a common origin, the coordinate transformation $Z = x \sin \alpha + z \cos \alpha$ simplifies to $Z = z/\cos \alpha$ because $x = z \tan \alpha$.

Assuming $\varepsilon \ll 1$, terms of order ε and ε^2 in (6) generally may be neglected. Then (6) reduces to a simple equation describing steady, near-surface groundwater flow [*Hurley and Pantelis*, 1985]

$$\frac{\partial}{\partial z^*}\left[K_z^*\left(\frac{\partial \psi^*}{\partial z^*} - \cos \alpha\right)\right] = 0. \tag{7}$$

A general solution of (7) is (in dimensional form)

$$\psi = z[\cos \alpha + f(x, y)(K_{sat}/K_z)] + c, \tag{8}$$

where c is a constant of integration that depends on water table depth and f is a function that depends on the rate and spatial distribution of long-term rain infiltration. Both c and f can be evaluated explicitly if appropriate boundary conditions are specified. Patterns of groundwater flow may be inferred from (8) by combining it with the definition of total head h, which yields

$$h = \psi - Z = -x \sin \alpha + zf(x, y)(K_{sat}/K_z) + c, \tag{9}$$

where the elevation head $Z = x \sin \alpha + z \cos \alpha$ is measured vertically downward from a horizontal reference plane that passes through the origin on the ground surface (Figure 3).

Some special cases of (8) and (9) warrant particular attention owing to their frequent use in applications. For example, if the long-term average infiltration rate in the z direction at the ground surface I_z is specified by a constant flux boundary condition $I_z = -K_z(\partial h/\partial z)$, and if the soil is homogenous, then the pressure head and total head below the water table (where $\psi = 0$) obey [cf. *Iverson*, 1990]

$$\psi = (z - d)[\cos \alpha - (I_z/K_z)], \tag{10a}$$

$$h = -x \sin \alpha - d \cos \alpha - (z - d)(I_z/K_z), \tag{10b}$$

where d is the water table depth measured normal to the ground surface. If infiltration is sufficiently slow that $I_z/K_z \ll \cos \alpha$, (10a) and (10b) reduce further to forms that describe slope-parallel groundwater flow

$$\psi = (z - d) \cos \alpha, \tag{11a}$$

$$h = -x \sin \alpha - d \cos \alpha. \tag{11b}$$

Equations (11a) and (11b) indicate that saturated groundwater flow in response to slow infiltration occurs only in the x direction, driven by the head gradient $\partial h/\partial x = -\sin \alpha$. The associated groundwater flux above a reference depth $z = \delta$ can be calculated by combining this head gradient with Darcy's law for flow in the x direction, yielding

$$Q_x = b(\delta - d) K_x \sin \alpha, \tag{12}$$

where Q_x is volumetric groundwater discharge in the x direction, b is the width (in the y direction) of the slope element over which Q_x is measured, K_x is the saturated hydraulic conductivity in the x direction, and $\delta - d$ is the water table height above the reference depth δ.

In utilizing (12), investigators commonly invoke mass conservation of groundwater by assuming that the flow domain is bounded by an impermeable bed at depth δ, but this approach can yield self-contradictory results. To see the contradiction, first consider slow variation of Q_x in response to slow infiltration ($I_z/K_z \ll \cos \alpha$). In such circumstances, (12) can be combined with the depth-averaged mass conservation equation $\partial Q_x/\partial A + \partial(\delta - d)/\partial t = I_z$ to form a kinematic wave model of slope-parallel groundwater flow, which applies over long timescales ($t \sim A/D_0$) [cf. *Beven*, 1981; *Hurley and Pantelis*, 1985; *Wu and Sidle*, 1995]. For still longer timescales ($t \gg A/D_0$), time dependence becomes negligible, and the kinematic wave mass conservation equation reduces to a steady discharge equation $Q_x = I_z A$, which can be combined with (12) to predict the steady water table height above the impermeable bed

$$\delta - d = \frac{I_z}{K_x} \frac{A}{b \sin \alpha}. \tag{13}$$

Equation (13) is the steady groundwater flow model used by *Montgomery and Dietrich* [1994] and *Dietrich et al*. [1995] to evaluate landslide susceptibility. Corresponding pressure head and total head distributions are found by solving (13) for d and combining the result with (11a) and (11b). The resulting equations

$$\psi = (z - \delta) \cos \alpha + \frac{I_z}{K_x} \frac{A}{b} \cot \alpha, \tag{14a}$$

$$h = -x \sin \alpha - \delta \cos \alpha + \frac{I_z}{K_x} \frac{A}{b} \cot \alpha \tag{14b}$$

reveal a paradox. If $I_z/K_x \to 0$, (14a) predicts negative pressure heads at depths $z < \delta$, which contradict the positive water table heights given by (13), yet the assumption $I_z/K_z \to 0$ is necessary to derive both (13) and (14a). To eliminate this paradox, one must assume strongly anisotropic conductivity, $K_z \gg K_x$ (which yields $I_z/K_x \gg I_z/K_z$), a condition not typical of many slopes.

In summary, equations for steady, slope-parallel groundwater flow above an impermeable bed (e.g., equations (13), (14a), and (14b)) can predict groundwater pressures produced by rainfall only if four conditions are satisfied: (1) The rainfall duration is very long ($t \gg A/D_0$), (2) the depth H is relatively small ($\varepsilon \ll 1$), (3) the rainfall intensity is very low ($I_z/K_z \ll \cos \alpha$), and (4) the slope-normal component of hydraulic conductivity greatly exceeds the slope-parallel component ($K_z \gg K_x$). Typically these conditions do not exist. Therefore I use

more general equations (such as (10a) and (10b)) and alternative approximations (valid for short-term, transient rainfall) to assess hydrologic conditions that trigger landslides.

2.2. Short-Term Behavior

Short-term piezometric responses to rainfall can be assessed by identifying the appropriate dimensionless time as $t^* = tD_0/H^2$ and substituting this expression together with (2), (3), and (4) into (1). Then multiplication of all terms by H/K_{sat} and some algebraic simplification yields a form of Richards equation appropriately scaled to assess $\psi(x, y, H, t)$ in response to rainfall of short duration ($t \ll A/D_0$)

$$\frac{C(\psi)}{C_0}\frac{\partial\psi^*}{\partial t^*} = \varepsilon^2\frac{\partial}{\partial x^*}\left[K_L^*\left(\frac{\partial\psi^*}{\partial x^*} - \frac{1}{\varepsilon}\sin\alpha\right)\right] + \varepsilon^2\frac{\partial}{\partial y^*}\left[K_L^*\left(\frac{\partial\psi^*}{\partial y^*}\right)\right] + \frac{\partial}{\partial z^*}\left[K_z^*\left(\frac{\partial\psi^*}{\partial z^*} - \cos\alpha\right)\right]. \quad (15)$$

Assuming $\varepsilon \ll 1$, terms of order ε and ε^2 in (15) generally may be neglected. Then (15) reduces to an equation describing near-surface groundwater flow in the z direction

$$\frac{C(\psi)}{C_0}\frac{\partial\psi^*}{\partial t^*} = \frac{\partial}{\partial z^*}\left[K_z^*\left(\frac{\partial\psi^*}{\partial z^*} - \cos\alpha\right)\right]. \quad (16)$$

This equation may be expressed in terms of a vertical coordinate $Z^* = x^*\sin\alpha + z^*\cos\alpha$ (defined as positive downward as in Figure 3) as

$$\frac{C(\psi)}{C_0}\frac{\partial\psi^*}{\partial t^*} = \cos^2\alpha\frac{\partial}{\partial Z^*}\left[K_z^*\left(\frac{\partial\psi^*}{\partial Z^*} - 1\right)\right], \quad (17)$$

which is the standard Richards equation for vertical infiltration, written in a normalized form that accounts for the effect of the surface slope α. This equation governs transient pressure head responses at depths that are relatively shallow ($\varepsilon \ll 1$) and times that are relatively short ($t \ll A/D_0$), but nonlinearity of the equation makes it difficult to solve analytically.

Analysis is facilitated by considering limiting forms of (17) that describe pressure head responses in soils that are initially either quite wet or quite dry. These limiting forms can be identified by differentiating the terms in brackets in (17) and using the definition of total head $h = \psi - Z$ in conjunction with Darcy's law for vertical flow in response to infiltration, $I_Z = -K_Z(\partial h/\partial Z)$, to rewrite (17) in a form that contains distinct gravity flux and pressure diffusion terms on the right-hand side

$$\frac{C(\psi)}{C_0}\frac{\partial\psi^*}{\partial t^*} = \cos^2\alpha\left[K_z^*\frac{\partial^2\psi^*}{\partial Z^{*2}} - \frac{I_Z}{K_Z}\frac{\partial K_z^*}{\partial Z^*}\right]. \quad (18)$$

Equation (18) indicates that if soils are sufficiently wet that $K_z \to K_{sat}$ and $C(\psi) \to C_0$, the gravity flux term involving I_Z/K_Z can be neglected, yielding a pressure head diffusion equation

$$\frac{\partial\psi^*}{\partial t^*} = \frac{C_0K_z^*\cos^2\alpha}{C(\psi)}\frac{\partial^2\psi^*}{\partial Z^{*2}}, \quad (19)$$

in which the normalized diffusivity is $(C_0K_z^*\cos^2\alpha)/C(\psi)$. On the other hand, if soils are sufficiently dry that $K_z \ll K_{sat}$ (i.e., $K_z^* \to 0$), the diffusion term in (18) can be neglected, and only the gravity flux term can be retained. Then (18) reduces to a kinematic wave equation, obtained by employing the chain rule $\partial K_z^*/\partial Z^* = (dK_z^*/d\psi^*)(\partial\psi^*/\partial Z^*)$ and rearranging terms to yield

$$\frac{\partial\psi^*}{\partial t^*} + \Gamma\frac{\partial\psi^*}{\partial Z^*} = 0, \quad (20)$$

where

$$\Gamma = \cos^2\alpha\frac{I_Z}{K_Z}\frac{C_0}{C(\psi)}\frac{dK_z^*}{d\psi^*} \quad (21)$$

is the normalized kinematic wave speed. The simplest nontrivial solution of (20)

$$\psi^* = \Gamma t^* - Z^* \quad (22)$$

predicts negative pressure heads where $Z^* > \Gamma t^*$ and positive pressure heads where $Z^* < \Gamma t^*$. Consequently, $Z^* = \Gamma t^*$ defines the location of a saturated wetting front that moves downward at the kinematic wave speed. As noted by *Smith and Hebbert* [1983], kinematic wave models of infiltration describe propagation of piston wetting fronts similar to that conceived in *Green and Ampt*'s [1911] model of infiltration.

A measure of the relative efficacy of piston front wetting and pore pressure diffusion during infiltration is provided by the ratio κ of the normalized kinematic wave speed in (21) to the normalized diffusivity in (19)

$$\kappa = \frac{I_Z}{K_Z}\frac{H}{K_z}\frac{dK_z}{d\psi}. \quad (23)$$

This expression for κ can also be obtained by writing (19) and (21) in dimensional form and dividing the timescale for pore pressure diffusion by the timescale for kinematic wave propagation. Small values of κ indicate the primacy of diffusion and apply most commonly when soils are relatively wet initially [cf. *Van Genuchten*, 1980]. To analyze conditions most prevalent when rainfall triggers landslides, I focus on wet initial conditions and assume that $\kappa \ll 1$ and equation (19) applies. However, (20) may be a better approximation if soils are dry before rainfall commences.

For wet initial conditions I assume $K_z \approx K_{sat}$, $C \approx C_0$, and that (19) consequently reduces to the approximation (in dimensional form) [cf. *Eagleson*, 1970, pp. 291–295]

$$\frac{\partial\psi}{\partial t} = D_0\cos^2\alpha\frac{\partial^2\psi}{\partial Z^2}. \quad (24)$$

Linearity of (24) allows superposition of solutions. Thus to evaluate pressure head responses to complicated rainfall sequences with varying intensities and irregular durations, it is necessary only to obtain a fundamental solution of (24) that describes the response $\psi(Z, t)$ to rainfall of fixed intensity and duration and to sum a series of responses.

An appropriate fundamental solution of (24) obeys the initial and boundary conditions

$$\psi(Z, 0) = (Z - d_Z)\beta, \quad (25a)$$

$$\frac{\partial\psi}{\partial Z}(\infty, t) = \beta, \quad (25b)$$

$$\frac{\partial\psi}{\partial Z}(0, t) = \begin{cases} -I_Z/K_Z + \beta & t \le T \\ \beta & t > T, \end{cases} \quad (25c)$$

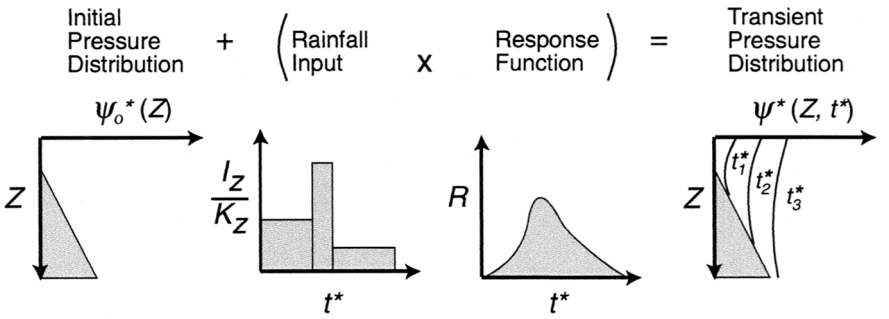

Figure 4. Schematic of rainfall input and pressure head response as described by equations (25a)–(25c), (26a)–(26c), and (27a)–(27e).

where T is the rainfall duration and the initial condition (25a) assumes a steady state pressure head distribution like that given in (10a). This distribution is conveniently expressed in terms of a steady water table depth d_Z (measured in the Z direction), and a constant β, where $\beta = \cos^2 \alpha - (I_Z/K_Z)_{\text{steady}}$. Here $(I_Z/K_Z)_{\text{steady}} = (I_z/K_z) \cos \alpha$ is the Z component of the normalized steady state water table recharge rate that appears in (10a); typically, $(I_Z/K_Z)_{\text{steady}}$ is much smaller than the normalized transient rainfall infiltration rate I_Z/K_Z. Simpler expressions for β can be employed for special steady states such as those with hydrostatic pressures ($\beta = 1$) or slope-parallel groundwater flow ($\beta = \cos^2 \alpha$). In general, however, these simplifications need not apply.

The constant β also appears in the boundary conditions (25b) and (25c). The lower boundary condition (25b) states that at great depths below the water table, transient vertical groundwater flux decays to zero and steady state pressures described by (10a) persist. The upper boundary condition (25c) states that Darcy's law governs water entry at the ground surface ($Z = 0$), where steady, background infiltration rates are determined by β and transient, short-term infiltration rates are I_Z if $t \le T$ and are zero if $t > T$. The condition $I_Z/K_Z = 1$ defines the maximum infiltration rate. If rainfall intensities exceed this rate, the surplus rainfall runs off as Horton overland flow.

The solution of the initial boundary value problem posed by (24) and (25a)–(25c) can be obtained by generalizing an analogous heat conduction solution described by *Carslaw and Jaeger* [1959, pp. 75–76], yielding

$$\psi(Z, t \le T) = (Z - d)\beta + \frac{I_Z}{K_Z}\left[\left(\frac{\hat{D}t}{\pi}\right)^{1/2} \exp\left(-\frac{Z^2}{\hat{D}t}\right) - Z \operatorname{erfc}\left(\frac{Z^2}{\hat{D}t}\right)^{1/2}\right], \quad (26a)$$

$$\psi(Z, t > T) = \psi(Z, t \le T) - \frac{I_Z}{K_Z}\left[\left(\frac{\hat{D}(t - T)}{\pi}\right)^{1/2} \exp\left(-\frac{Z^2}{\hat{D}(t - T)}\right) - Z \operatorname{erfc}\left(\frac{Z^2}{\hat{D}(t - T)}\right)^{1/2}\right], \quad (26b)$$

in which

$$\hat{D} = 4D_0 \cos^2 \alpha \quad (26c)$$

is an effective hydraulic diffusivity and erfc is the complementary error function. Equation (26a) applies while rainfall continues ($t \le T$), whereas (26b) applies after rainfall stops ($t > T$).

Significant simplification of (26a) and (26b) results from normalization with respect to Z. Division of all terms in (26a) and (26b) by Z yields

$$\frac{\psi}{Z}(Z, t \le T) = \beta(1 - d/Z) + \frac{I_Z}{K_Z}[R(t^*)], \quad (27a)$$

$$\frac{\psi}{Z}(Z, t > T) = \beta(1 - d/Z) + \frac{I_Z}{K_Z}[R(t^*) - R(t^* - T^*)], \quad (27b)$$

in which

$$t^* = \frac{t}{Z^2/\hat{D}}, \quad (27c)$$

$$T^* = \frac{T}{Z^2/\hat{D}} \quad (27d)$$

are normalized times and

$$R(t^*) = \sqrt{t^*/\pi} \exp(-1/t^*) - \operatorname{erfc}(1/\sqrt{t^*}) \quad (27e)$$

is a pressure head response function, which depends only on normalized time.

Equations (27a)–(27e) indicate that calculation of groundwater pressure heads at all depths Z and all times t^* requires only knowledge of the pressure head response function $R(t^*)$ and three additional kinds of information: an initial (steady state) pressure head distribution (given by (10a) and represented by the first term on the right-hand sides of (27a) and (27b)) and a normalized rainfall intensity I_Z/K_Z and duration T^* (Figure 4). This economy of information requirements and computational demands makes rapid application of (27a)–(27e) over broad regions feasible.

2.3. Hydrologic Responses

Figures 5 and 6 illustrate key features of the pressure head response function $R(t^*)$ for $t^* \le T^*$ and $R(t^*) - R(t^* - T^*)$ for $t^* > T^*$. Figure 5 depicts graphs of the function for three rainfall durations that span a range of great practical interest, $T^* = 0.1$, 1, and 10. (For example, if $Z = 2$ m and $\hat{D} = 10^{-4}$ m^2/s, these durations correspond to ~1, 10, and 100 hours.) For all rainfall durations the response remains close to zero until about $t^* = 0.2$, then increases smoothly and continues to increase until briefly after rainfall ceases (as a result of pressure head redistribution) and peaks at a value R_{peak} at time t^*_{peak}. After peaking, the response gradually declines and asymptotically approaches zero. For rainfall durations $T^* \le 1$, responses exhibit a nearly constant shape and time to peak,

$t^*_{peak} \sim 2$, and response magnitudes vary in almost exact proportion to T^* (Figures 5a and 5b). For rainfall durations $T^* > 1$, peak responses occur sooner after rainfall ceases and have somewhat smaller magnitudes relative to T^* (Figures 5b and 5c).

Figure 6 illustrates how the peaking behavior depicted in Figure 5 varies as a function of rainfall duration T^*. The curves in Figure 6 demonstrate that a systematic change in peaking behavior occurs between $T^* = 1$ and $T^* = 10$ (compare Figure 5). This change reflects trade-offs between pressure head propagation and attenuation that occur as rainfall input becomes less abrupt and more continuous. For rainfall inputs longer than $T^* \sim 10$, R_{peak} approaches $T^*/20$ (Figure 6). This unbounded growth of R_{peak} with growth of T^* demonstrates that transient pressure diffusion solutions provide unrealistic predictions of long-term (approximately steady state) pressure heads that develop in response to persistent rainfall. Steady state pressure heads are described better by an equation such as (10a).

Figures 7 and 8 show examples of pressure head distributions predicted by (27a)–(27e) for two well-documented landslides with contrasting soil, slope, and rainfall properties (summarized in Table 2). Together, Figures 7 and 8 illustrate the profound influence of hydraulic diffusivity and rainfall intensity and duration on transient pressure head responses that may trigger slope failure. Figures 7 and 8 also demonstrate that the fastest and largest pressure head responses always occur near the ground surface, with more subdued and delayed responses at depth. After rainfall ceases, pressure heads slowly relax to near–steady state gradients but, for a long time, remain elevated above those of the initial steady state (as dictated by the slowly declining tail of the response function shown in Figure 5).

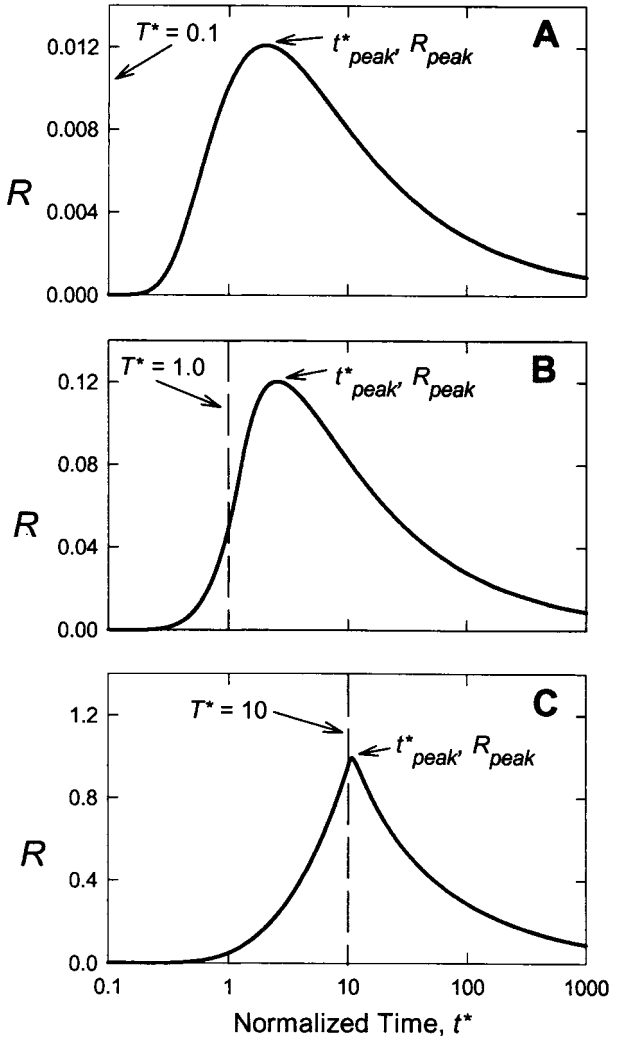

Figure 5. Graphs of the pressure head response function R for three normalized rainfall durations $T^* = 0.1$, 1, and 10. Graphs depict $R(t^*)$ for $t^* \le T^*$ and $R(t^*) - R(t^* - T^*)$ for $t^* > T^*$.

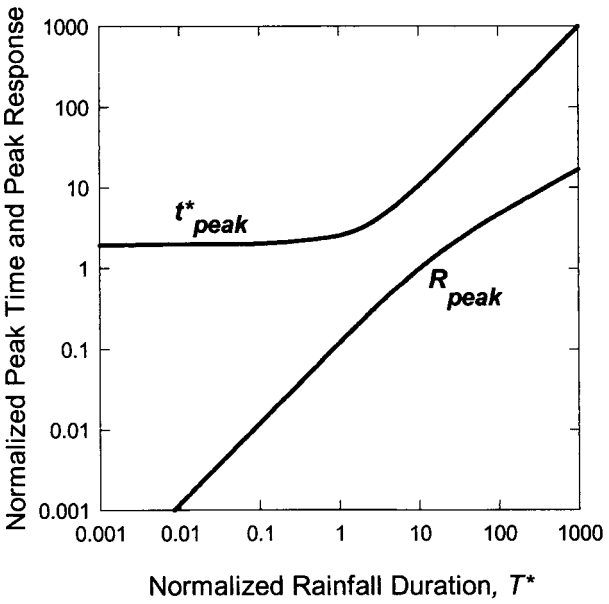

Figure 6. Graphs of the peaking behavior of the pressure head response function (Figure 5) for a wide range of normalized rainfall durations. Graphs of the time to peak (t^*_{peak}) and magnitude of the peak response (R_{peak}) were constructed by evaluating $R(t^*) - R(t^* - T^*)$ for a range of T^*.

Figure 7 illustrates pressure head responses typical of Minor Creek landslide, a seasonally active, slow-moving, clay-rich landslide in northern California [*Iverson*, 1984, 1986]. The landslide slopes 15°, has typical saturated hydraulic conductivities $\sim 5 \times 10^{-8}$ m/s and hydraulic diffusivities $\sim 10^{-6}$ m^2/s, and commonly receives ~ 2 m of rainfall distributed throughout a six-month rainy season [*Iverson and Major*, 1987]. The average wet season rainfall rate ($\sim 1 \times 10^{-7}$ m/s) exceeds typical saturated conductivities, so that $I_Z/K_Z = 1$. Although most of the landslide soil remains nearly saturated year-round, pore water pressures measured in the basal shear zone of the landslide (at 5–6 m depth) respond significantly to seasonal rainfall cycles but respond negligibly to rainfall cycles of less than a few months duration. As a consequence, the landslide accelerates each wet season but does not accelerate measurably in response to even the most intense individual storms [*Iverson*, 1984; *Iverson and Major*, 1987]. The predictions of Figure 7 mimic the hydrologic behavior at Minor Creek landslide under circumstances in which (1) an initial steady state water table exists at 2 m depth (similar to the observed dry season water table), (2) $D_0 = 10^{-6}$ m^2/s, (3) $I_Z/K_Z = 1$, and (4) rainfall of two different durations (10 days and 12 weeks) occurs. Figure 7a demonstrates that pressure heads at the landslide base (5–6 m depth) respond negligibly to the 10 day rainfall input,

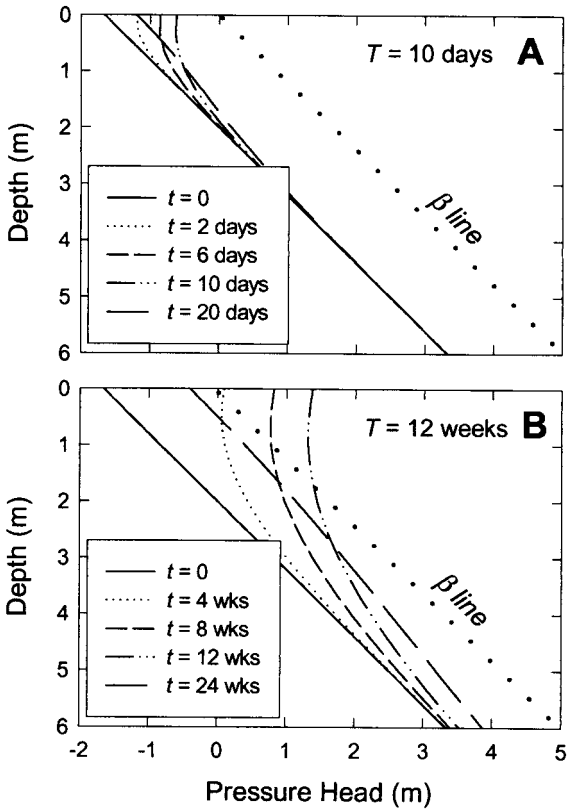

Figure 7. Pressure head responses predicted by equations (27a)–(27e) for conditions representative of the clay-rich Minor Creek landslide [*Iverson and Major*, 1987] for a normalized rainfall intensity $I_Z/K_Z = 1$ and contrasting rainfall durations (a) $T = 10$ days and (b) $T = 12$ weeks. Pressure heads above the β line are physically unrealistic and can be amended to equal $Z\beta$.

whereas Figure 7b demonstrates that responses to the 12 week rainfall input are considerable at this depth. Predicted pressure heads at the landslide base ultimately increase by ~1 m, similar to the observed pressure head changes that trigger seasonal landslide motion [*Iverson and Major*, 1987].

Figure 8 illustrates much faster pressure head responses predicted for landslide experiments like those described by *Iverson et al.* [1997] and *Reid et al.* [1997]. These experiments involve application of artificial rainfall to rectilinear prisms of 6 m^3 of soil placed behind a 65-cm-high retaining wall on a 31° concrete-lined slope. In some of these experiments the soil is prewetted by application of low-intensity rainfall to raise moisture contents to near-saturation levels without producing positive pressure heads [*Reid et al.*, 1997, experiments 2 and 3]. Higher-intensity rainfall (at rates of 180–400 mm/h) is then used to elevate groundwater pressures and trigger slope failure. A loose loamy sand used in recent (1998) versions of these experiments has $K_{sat} \sim 10^{-4}$ m/s and $D_0 \sim 10^{-3}$ m^2/s as it approaches saturation (Table 2). Thus rainfall at rates of 180 and 400 mm/h corresponds to $I_Z/K_Z \approx 0.5$ and $I_Z/K_Z \approx 1$, respectively. For $D_0 = 10^{-3}$ m^2/s and a rainfall duration $T = 10$ min, Figure 8 demonstrates that pressure head responses to these two rainfall intensities exhibit differing styles of behavior. Lower intensity rainfall (Figure 8a) causes gradual water table accretion from the bottom up, and pressure head gradients both above and below the water table deviate relatively little from steady state gradients. This behavior is similar to that observed by *Iverson et al.* [1997] and *Reid et al.* [1997] in moderate-intensity rainfall experiments. In contrast, higher-intensity rainfall (Figure 8b) causes positive pressure heads to develop quite suddenly (at about $t = 6$ min) and almost simultaneously at a range of depths. This behavior is similar to that inferred by *Reid et al.* [1997] for high-intensity rainfall experiments and by *Torres et al.* [1998] for the Coos Bay field site listed in Table 1, and it mimics behavior produced by rainfall on tension-saturated soil [*Gillham*, 1984].

Figures 7b and 8b also show that pressure heads predicted for the shallowest depths can eventually rise to unrealistically high levels. These pressure heads exceed values denoted by a "β" line, which indicates maximum pressure heads sustainable with a water table at the ground surface and the steady, background, vertical flow components $(I_Z/K_Z)_{steady}$ listed in Table 2. Prediction of unrealistic pressure heads at shallow depths results from the constant flux boundary condition (25c) and lack of a gravity drainage term in the linear pressure diffusion model (24). For the analyses of landsliding described in section 3, pressure head predictions for shallow depths are restricted by specifying that pressure heads cannot exceed those given by the β line, $\psi = Z\beta$ (compare equations (25a)–(25c) and Figures 7 and 8). This restriction is rather ad hoc but is necessary when using a linear model and constant flux boundary to approximate the nonlinear effects of rainfall infiltration.

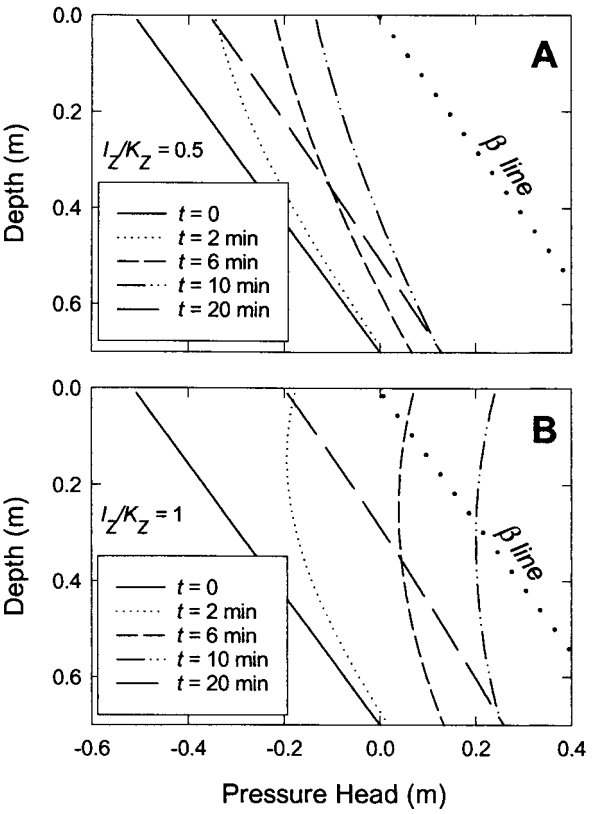

Figure 8. Pressure head responses predicted by equations (27a)–(27e) for conditions representative of sandy loam landslide experiments similar to those reported by *Iverson et al.* [1997] and *Reid et al.* [1997] for a rainfall duration $T = 10$ min and contrasting rainfall intensities (a) $I_Z/K_Z = 0.5$ and (b) $I_Z/K_Z = 1$. Pressure heads above the β line are physically unrealistic and can be amended to equal $Z\beta$.

Table 2. Slope, Soil, and Rainfall Properties Used to Generate Figures 7, 8, 10, 11, 12, and 13

Property, Symbol, and Unit	Minor Creek Landslide	Landslide Experiment, June 23, 1998
Slope properties		
Slope angle (α), deg	15	31
Landslide depth, vertical (Z), m	6	0.4
Steady state water table depth, vertical (d_Z), m	2	0.7 (concrete bed depth)
Steady state vertical water influx $(I_Z/K_Z)_{\text{steady}}$	0.1	0
Soil properties		
Soil composition	in situ gravely clay	reconstituted loamy sand
Friction angle (φ), deg	18 (residual)	38 (peak)
Cohesion (c), Pa	4000	500
Soil unit weight, wet (γ_s), N/m^3	22,000	19,000
Pore water unit weight (γ_w), N/m^3	9800	9800
Hydraulic conductivity (K_{sat}), m/s	5×10^{-8}	1×10^{-4}
Hydraulic diffusivity (D_0), m^2/s	1×10^{-6}	1×10^{-3}
Rainfall properties		
Rainfall intensity, vertical (I_Z), m/s	1×10^{-7} (6 cm/week)	5×10^{-5} (18 cm/hour), 1×10^{-4} (40 cm/h)
Rainfall duration (T), s	864,000 (10 days), 7,257,600 (12 weeks)	600 (10 min)
Normalized properties		
Normalized infiltration rate, vertical (I_Z/K_Z)	1	0.5, 1
Normalized rainfall duration (T^*)	0.09, 0.8	11
S (equation (33b))	1.2×10^7	270

More detailed descriptions of the two landslide scenarios summarized here are provided by *Iverson* [1984, 1986], *Iverson and Major* [1987], *Iverson et al.* [1997], and *Reid et al.* [1997].

3. Analysis of Landslide Processes

Landsliding involves two basic phenomena, slope failure and postfailure motion, which I analyze sequentially. Both analyses assume that groundwater flow established over times longer than A/D_0 produces a steady, background pressure head distribution $\psi_0(x, y, Z)$ described by an equation such as (10a). In addition, the analyses consider the effects of transient pressure heads (which change over times much less than A/D_0) due to infiltrating rain. These pressure changes are assumed to obey (27a)–(27e) and to influence both slope failure and postfailure motion.

3.1. Slope Failure

To evaluate the potential for slope failure at diverse locations within a landscape, I use a one-dimensional infinite-slope stability analysis, which neglects all forces not resolvable on planes that parallel the ground surface (Figure 9). An infinite-slope geometry is a rigorous, lowest-order approximation of a multidimensional landslide geometry if $H \ll L$, where H is the prospective slip surface depth and L is the prospective landslide length or width. The assumption $H \ll L$ is also compatible with the assumption $\varepsilon \ll 1$ used to develop the Richards equation approximations (7) and (16) of groundwater flow in slopes. A related idiosyncracy of infinite-slope analyses results from the need to specify a maximum plausible failure depth H. Without this specification no bound exists for landslide thickness. Commonly, a practical upper bound for H can be identified on the basis of geological stratification in which strong rock underlies a weaker overburden.

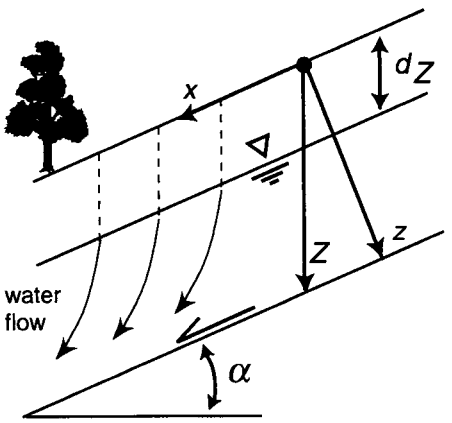

Figure 9. Schematic illustrating the infinite-slope model of slope stability, which assumes no variation of any quantity in the x direction or the direction normal to the page.

Incipient failure of infinite slopes is described by an equation that balances the downslope component of gravitational driving stress against the resisting stress due to basal Coulomb friction (mediated by pore water pressure). Failure occurs at depth Z (measured vertically from the origin such that $Z = z/\cos\alpha = x \sin\alpha + z \cos\alpha$; Figures 3 and 9) if at that depth

$$FS = F_f + F_w + F_c = 1, \tag{28a}$$

where the dimensionless "factor of safety" FS has components [*Iverson*, 1991]

$$F_f = \frac{\tan\varphi}{\tan\alpha}, \tag{28b}$$

$$F_w = \frac{-\psi(Z, t)\gamma_w \tan\varphi}{\gamma_s Z \sin\alpha \cos\alpha}, \tag{28c}$$

$$F_c = \frac{c}{\gamma_s Z \sin\alpha \cos\alpha} \tag{28d}$$

and φ is the soil friction angle, c is the soil cohesion, γ_s is the depth-averaged soil unit weight, and γ_w is the unit weight of groundwater. Equations (28a)–(28d) avoid the assumption of slope-parallel groundwater flow, which is unnecessary and inappropriate if significant rainfall infiltration occurs [*Iverson*, 1990, 1991]. Instead, the pressure head distribution $\psi(Z, t)$ in (28c) determines groundwater effects on slope stability. The position of the water table is irrelevant mechanically (except

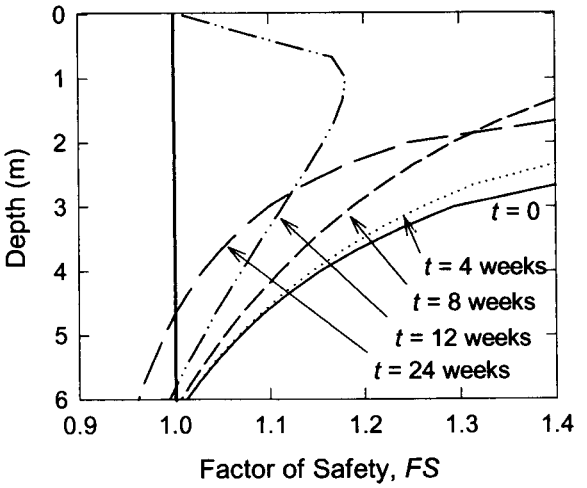

Figure 10. Factors of safety predicted by equations (29a)–(29c) using the pressure head distributions for Minor Creek landslide depicted in Figure 7b (T = 12 weeks, I_Z/K_Z = 1) in combination with soil mechanics parameters summarized in Table 2.

insofar as it might subtly influence γ_s) if the pressure head distribution is known.

When rainfall occurs, the factor of safety defined by (28a)–(28d) varies as a function of depth and time, and it is convenient to split the factor of safety into a time-varying component FS' and steady background component FS_0, as envisaged by *Terzaghi* [1950],

$$FS(Z, t) = FS_0(Z) + FS'(Z, t), \tag{29a}$$

$$FS_0(Z) = F_f + F_c - \frac{\psi_0(Z)\gamma_w \tan \varphi}{\gamma_s Z \sin \alpha \cos \alpha}, \tag{29b}$$

$$FS'(Z, t) = -\frac{[\psi(Z, t) - \psi_0(Z)]\gamma_w \tan \varphi}{\gamma_s Z \sin \alpha \cos \alpha}. \tag{29c}$$

If the steady, background pressure head distribution $\psi_0(Z)$ is known (e.g., from equations (10a) and (10b)), and if appropriate values of the slope and soil parameters α, φ, c, γ_s, γ_w are known, then the background factor of safety FS_0 can be calculated for every depth Z. Such calculations follow the conventions of typical steady state analyses of slope stability.

The time-varying component of the factor of safety at every depth Z is obtained by combining (29c) with (27a)–(27e), which yields

$$FS'(Z, t) = -\frac{\gamma_w}{\gamma_s} \frac{\tan \varphi}{\sin \alpha \cos \alpha} \frac{I_Z}{K_Z} \cdot \begin{cases} [R(t^*)] & t^* \le T^* \\ [R(t^*) - R(t^* - T^*)] & t^* > T^*. \end{cases} \tag{30}$$

Equation (30) demonstrates that $FS'(Z, t)$ depends on only three dimensionless variables (time t^*, rainfall duration T^*, and rainfall intensity I_Z/K_Z) in addition to the soil and slope parameters that determine the steady, background factor of safety FS_0. Therefore to account for transient rainfall effects, the only information that must be added to a steady state analysis is the rainfall intensity and duration and the timescale $Z^2/\hat{D}$. Moreover, it is unnecessary to specify the depth of slope failure, because the analysis of failure mechanics combined with transient groundwater pressure heads predicts factors of safety at all depths Z. The depth Z that first yields FS = 1 determines the depth of landsliding, which may vary in response to different rainfall inputs.

Figures 10 and 11 depict factors of safety $FS(Z, t)$ calculated from (29a)–(29c) using the pressure head conditions depicted in Figures 7b and 8b (amended to restrict pressure heads to values no higher than the β line). Table 2 summarizes the soil mechanics parameters used for each calculation (derived from independent measurements reported by *Iverson and Major* [1987] and *Iverson et al.* [1997]). The results shown in Figures 10 and 11 illustrate the great range of conditions that can lead to rainfall-triggered landsliding. Not only does the timing of landsliding illustrated in the two figures differ by many orders of magnitude, but the style of the rainfall trigger differs as well.

Figure 10 predicts that seasonal motion of Minor Creek landslide results from slow pressure head increases and gradual water table accretion, as described by *Iverson and Major* [1987]. The condition FS = 1 is satisfied first at the landslide base (~6 m depth) and slowly spreads upward. Factors of safety do not drop much below 1, however: a condition that favors slow landslide motion if soil resistance increases slightly with increasing deformation.

In contrast, Figure 11 predicts that during intense rainfall on prewetted sandy soils, slope failure can result from positive pressure heads that develop first near the ground surface and spread rapidly downward. Scenarios like that shown in Figure 11 favor abrupt triggering of shallow landslides as described by *Reid et al.* [1997], rather than deeper-seated landsliding due to water table accretion.

3.2. Postfailure Motion

Postfailure movement of a translating landslide mass depends, in part, on soil properties that may cause deforming soil to progressively weaken or strengthen [*Leroueil and Marques*, 1996]. However, the interplay of subsurface hydrology and landslide inertia also plays a role, which is the focus here. For a landslide of arbitrary thickness Z the effect of inertia can be

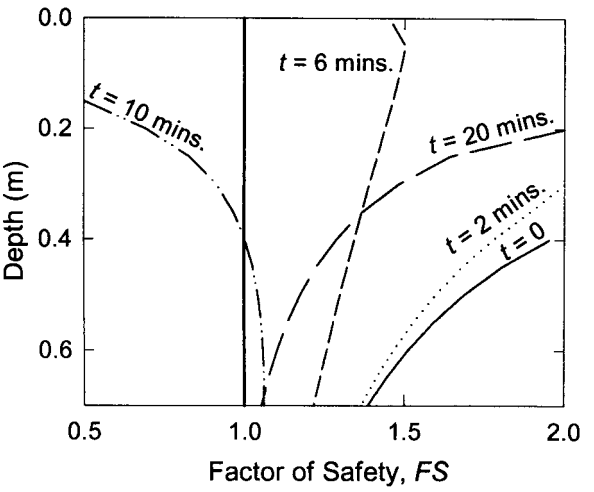

Figure 11. Factors of safety predicted by equations (29a)–(29c) using the pressure head distributions for sandy soil landslide experiments depicted in Figure 8b (T = 10 min, I_Z/K_Z = 1) in combination with soil mechanics parameters summarized in Table 2.

evaluated by modifying (28a)–(28d) to account for the acceleration term in Newton's second law, yielding an equation of motion [cf. *Iverson et al.*, 1997]

$$\frac{1}{g}\frac{dv}{dt} = \sin\alpha[1 - FS(Z, t)], \tag{31}$$

where v is downslope landslide velocity and g is the magnitude of gravitational acceleration. Of course, equation (31) applies only after $FS(Z, t) < 1$ is satisfied. The equation can be generalized to account for internal deformation [*Iverson*, 1997], but translational sliding rather than internal deformation is the present focus.

By combining (29a)–(29c), (30), and (31) the landslide equation of motion can be written in a form that separates the steady background factor of safety $FS_0(Z)$ from the time-varying component $FS'(Z, t)$. Then expressing $FS'(Z, t)$ in terms of the response function R yields

$$\frac{1}{g}\frac{dv}{dt} = \sin\alpha[1 - FS_0(Z)] + \frac{\gamma_w}{\gamma_s}\frac{\tan\varphi}{\cos\alpha}\frac{I_Z}{K_Z} \cdot \begin{cases} [R(t^*)] & t^* \le T^* \\ [R(t^*) - R(t^* - T^*)] & t^* > T^*, \end{cases} \tag{32}$$

which applies only after the right-hand side exceeds 0. The right-hand side cannot exceed 0 under steady state hydrologic conditions, because the first term on the right-hand side of (32) is always negative and the second term is zero at steady state. Solution of (32) also requires an initial condition for landslide velocity, typically $v = 0$ at $t = 0$.

Before solutions of (32) can be generated, an important timescale discrepancy must be rectified. Time variables on the right-hand side of (32) are normalized by the diffusion timescale $Z^2/\hat{D}$, whereas the left-hand side of (32) involves dimensional time t. To eliminate this discrepancy, I define the normalized landslide velocity as $v^* = v/\sqrt{Zg}$ and rewrite (32) as

$$\frac{dv^*}{dt^*} = S\sin\alpha[1 - FS_0(Z)] + S\frac{\gamma_w}{\gamma_s}\frac{\tan\varphi}{\cos\alpha}\frac{I_Z}{K_Z} \cdot \begin{cases} [R(t^*)] & t^* \le T^* \\ [R(t^*) - R(t^* - T^*)] & t^* > T^*, \end{cases} \tag{33a}$$

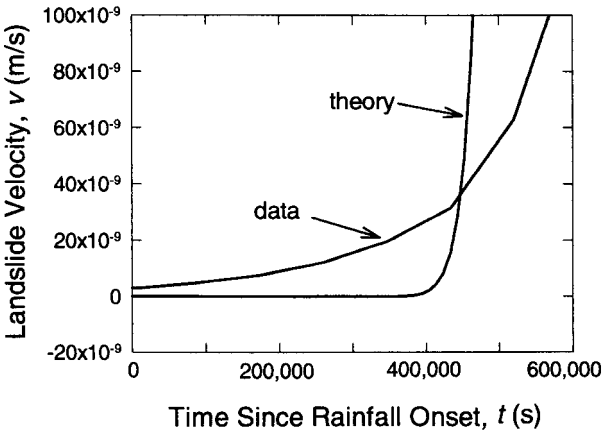

Figure 12. Measured and predicted velocity histories for Minor Creek landslide in November 1983. Measurements were described by *Iverson* [1984]. Predictions were generated by numerical integration of equation (33a) using $FS_0 = 1$, $I_Z/K_Z = 1$, and other parameter values summarized in Table 2.

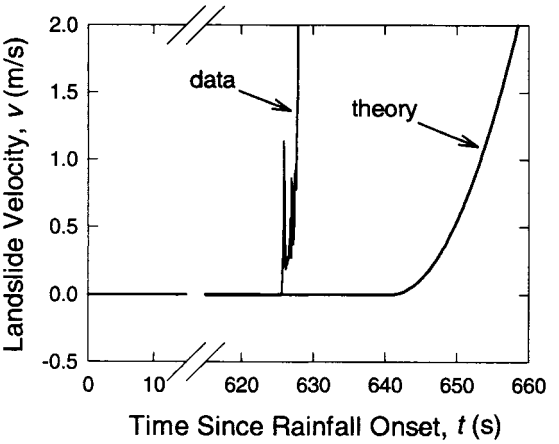

Figure 13. Measured and predicted velocity histories for landslide experiment, June 23, 1998, which was very similar to the high-intensity rainfall experiment described by *Reid et al.* [1997] but used a finer-grained soil. Predictions were generated by numerical integration of equation (33a) using $FS_0 = 2$, $I_Z/K_Z = 1$ and other parameter values summarized in Table 2.

where

$$S = \frac{Z^2/\hat{D}}{\sqrt{Z/g}} = \frac{Z^{3/2}g^{1/2}}{\hat{D}} \tag{33b}$$

is the ratio of the pore pressure diffusion timescale to the landslide acceleration timescale $\sqrt{Z/g}$. For typical values of Z (>1 m) and $\hat{D}$ ($<10^{-2}$ m^2/s), S exceeds 100, indicating that landslide acceleration can occur much more rapidly than pore pressure diffusion.

The contrast in timescales denoted by large values of S has important implications for computing solutions of (33a). Although (33a) can be integrated numerically using a standard technique such as Simpson's rule, normalized time steps Δt^* must be very small ($\Delta t^* \ll 1/S$) to resolve landslide motion accurately. This constraint implies that time steps must be extraordinarily small relative to the timescale for pore pressure diffusion. Fortunately, the analytical expression on the right-hand side of (33a) obviates iterative computation of pore pressure diffusion, and numerical integrations using Simpson's rule to find $v^*(t^*)$ proceed very rapidly.

Figures 12 and 13 compare predictions of the timing and speed of landslide motion obtained from (33a) with landslide surface velocity data obtained using recording extensometers. The figures demonstrate that greatly differing timescales and velocity scales can typify motion of landslides.

Figure 12 depicts conditions at Minor Creek landslide during the onset of wet season motion that began November 1, 1983 [*Iverson*, 1984]. Soil moisture storage during the unusually wet year that preceded November 1, 1983, was sufficient to maintain the landslide in an almost saturated state and to maintain FS very close to 1 at the landslide base (6 m depth) [*Iverson and Major*, 1987]. Consequently, model calculations assume that $FS_0 = 1$ when persistent seasonal rainfall begins (Figure 10). Landslide responses to this rainfall are gradual rather than abrupt. Both theory and measurements indicate that landslide accelerations occur on timescales of days ($\sim 10^5$ s) after motion commences. Theory predicts the timing of landslide motion reasonably well, and it predicts velocities of

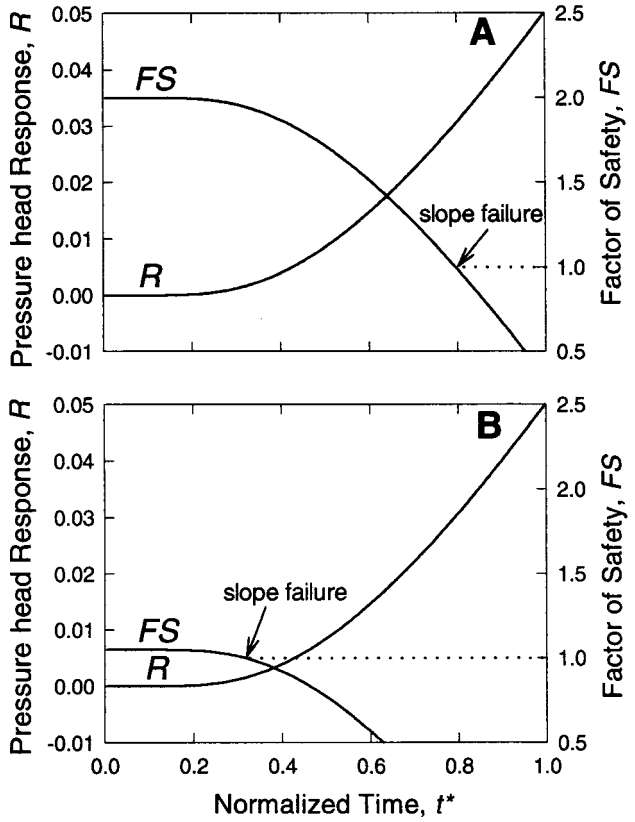

Figure 14. Relationships between pressure head responses (summarized by R), factors of safety (FS), and normalized time in contrasting landslides. Figures 14a and 14b both assume that rainfall of normalized duration $T^* = 1$ and fixed intensity begins at $t^* = 0$, but then assume that contrasting slope and soil properties produce significant differences in the initial factor of safety and growth of normalized time: Slope failure occurs during rapid changes in R and FS (Figure 14a); Slope failure occurs during gradual changes in R and FS (Figure 14b).

the correct order of magnitude, but it predicts accelerations that are somewhat too large. The discrepancy between theory and data might result from rate-dependent resistance (due to pore dilation and consequent strain hardening or due to rate-dependent friction), which are not included in the model [cf. *Iverson*, 1986].

Figure 13 depicts velocities measured during an artificial landslide experiment (June 23, 1998), which contrast sharply with velocities at Minor Creek landslide. In this experiment the sandy soil was prewetted to raise moisture contents to near-saturation levels, but pressure heads at all depths remained negative during prewetting, and the factor of safety remained high (~2) at the prospective failure depth of 0.4 m (Figure 11). Consequently $FS_0 = 2$ was used in (33a) to compute the timing and velocity of failure. Figure 13 demonstrates that the theory predicts the timing of failure remarkably well, and it correctly predicts the abrupt and rapid character of failure. However, the theory errs by underpredicting the landslide acceleration: an error opposite to that which arises in predicting Minor Creek landslide's acceleration. In the case of the June 23, 1998, landslide experiment, underprediction of acceleration probably results from undrained loading and strain weakening of the soil during slope failure. Strain weakening occurs because cohesive bonds break during failure and pores in the loosely packed soil contract during failure, transiently elevating pore water pressures and reducing frictional resistance [*Iverson et al.*, 1997]. Both contractile weakening of loose soils and dilatant hardening of dense soils can be incorporated in models of landslide motion, at the expense of additional complexity and data requirements.

4. Discussion

Figure 14 summarizes relationships between the hydrologic and landslide processes described above for two archetypical cases. The figure juxtaposes curves that show how pressure head responses $R(t^*)$ and factors of safety FS coevolve when rainfall of normalized duration $T^* = 1$ triggers different styles of landslides.

Shallow, rapid landslides commonly occur under conditions similar to those depicted in Figure 14a. Such landslides commonly involve thin, sandy soils on steep slopes, which yield small slip surface depths (Z) and large effective hydraulic diffusivities ($\hat{D}$). As a consequence, normalized time ($t^* = t\hat{D}/Z^2$) grows rapidly once rainfall commences, and pressure head responses $R(t^*)$ quickly reach a stage where they rise steeply (after $t^* \approx 0.3$ in Figure 14). Efficient drainage of the slope produces large FS values before rainfall commences ($FS_0 = 2$ in Figure 14a), but during intense rainfall, FS can decline rapidly owing to the steep pressure head increase. Slope failure occurs abruptly during rapid decline of FS, with rapid postfailure acceleration.

In contrast, slow-moving landslides commonly occur under conditions similar to those depicted in Figure 14b. Such landslides typically involve thick, relatively fine-grained soils that yield large slip surface depths (Z) and small effective hydraulic diffusivities ($\hat{D}$). As a consequence, normalized time ($t^* = t\hat{D}/Z^2$) proceeds slowly after rainfall commences, and pressure head responses $R(t^*)$ long remain confined to the region where they change very subtly (prior to $t^* \approx 0.3$ in Figure 14). Slow drainage of the slope tends to hold factors of safety not far above 1 during steady state conditions (assuming the slope is potentially unstable), and rainfall changes this situation only moderately. Thus if slope failure occurs, it occurs gradually in response to slight changes in the balance of forces.

The "rapid" and "slow" landslides characterized above represent archetypes, but intermediate cases are obviously possible. Nonetheless, distinctions between rapid and slow landslides are important owing to differing implications for landscape change and hazards. Rapid landslides can pose mortal dangers, whereas slow landslides destroy property but seldom cause fatalities.

5. Conclusions

Landslide responses to rainfall involve transient processes with different intrinsic timescales. A new model of these transient processes links slope failure and landslide motion to groundwater pressure heads that change in response to rainfall. The model requires little information in addition to that required by steady state models. New information needs consist of a hydraulic diffusivity D_0, rainfall intensity I_Z, and rainfall duration T (or a sequence of intensities and durations). The parsimony of these requirements results from use of five simplifying assumptions: (1) The prospective landslide thickness (H or Z), is much smaller than the square root of the

upslope groundwater contributing area A, so that $\varepsilon \ll 1$. (2) The rainfall duration T that triggers slope failure is much less than the steady state groundwater response time at the prospective landslide location, so that $T \ll A/D_0$. (3) The hydraulic diffusivity D_0 varies negligibly, which implies that soils are relatively wet before landslide-triggering rainfall commences. (4) Landslide mechanics can be represented adequately by an "infinite-slope" force balance that neglects all forces not resolvable on planes that parallel the ground surface. (5) Soil strength depends on constant Coulomb parameters, friction angle φ, and cohesion c.

Under these assumptions, landsliding triggered by rainfall obeys simple algebraic equations cast in terms of a normalized rainfall intensity I_Z/K_Z and response function $R(t^*) = \sqrt{t^*/\pi}\ \exp(-1/t^*) - \mathrm{erfc}(1/\sqrt{t^*})$ that depends only on normalized time $t^* = tD_0/Z^2$. This function predicts pressure head responses to rainfall, which, in turn, govern slope failure and postfailure landslide motion.

In some cases, pressure head growth and slope failure can occur rather abruptly in response to intense rainfall, and landslides can accelerate catastrophically. Such behavior is typical where shallow soils (with small Z) have high diffusivities (D_0). In such cases, normalized time proceeds rapidly after rainfall commences, and the pressure head response function R rises quickly.

In contrast, locations such as Minor Creek landslide (with thick soil and low hydraulic diffusivity) favor slow landsliding. In these cases, normalized time proceeds slowly, and the pressure head response function rises almost imperceptibly for a long time, even under sustained rainfall of high intensity. If landsliding occurs, it occurs gradually, with prolonged acceleration preceding any catastrophic movement.

The model developed here predicts key aspects of the behavior of "fast" and "slow" landslides, but it neglects factors that can be important. In particular, it neglects soil strength evolution, such as that due to contractile strain weakening, dilatant strain hardening, and fabric development, and it neglects mechanical effects of three-dimensional landslide geometries. Despite these shortcomings the model adds realism to current models that predict landsliding as a function of steady state hydrology, and it does so with a minimum of added data requirements. The model also provides information for assessing rates of postfailure landslide motion, thereby refining hazard forecasts.

Acknowledgments. Discussions with Mark Reid helped motivate this work. Comments by Mark Reid, Alan Howard, Gerald Wieczorek, and Stephen Lancaster helped improve the manuscript. Landslide experiments at the USGS debris flow flume benefitted from the participation of many people, especially Richard LaHusen, Matthew Logan, Mark Reid, Dianne Brien, Neal Iverson, and Janet Mann.

References

Baum, R. L., and M. E. Reid, Geology, hydrology and mechanics of a slow-moving, clay-rich landslide, Honolulu, Hawaii, in *Clay and Shale Slope Instability*, edited by W. C. Haneberg and S. A. Anderson, pp. 79–105, Geol. Soc. of Am., Boulder, Colo., 1995.

Bear, J., 1972, *Dynamics of Fluids in Porous Media*, Dover, Mineola, New York, 1972.

Beven, K., Kinematic subsurface stormflow, *Water Resources Research*, *17*, 1419–1424, 1981.

Biot, M. A., General theory of three-dimensional consolidation, *J. Appl. Phys*., *12*, 155–164, 1941.

Biot, M. A., Theory of propagation of elastic waves in a fluid-saturated porous solid, I, Low-frequency range, *J. Acoust. Soc. Am*., *28*, 168–178, 1956.

Caine, N., The rainfall intensity-duration control of shallow landslides and debris flows, *Geogr. Ann*., *Ser. A*, *62*, 23–27, 1980.

Cannon, S. H., and S. Ellen, Rainfall conditions for abundant debris avalanches in the San Francisco Bay region, California, *Calif. Geol*., *38*, 267–272, 1985.

Carslaw, H. S., and J. C. Jaeger, *Conduction of Heat in Solids*, Oxford Univ. Press, New York, 1959.

Chandler, R. N., and D. L. Johnson, The equivalence of quasi-static flow in fluid-saturated porous media and Biot's slow wave in the limit of zero frequency, *J. Appl. Phys*., *52*, 3391–3395, 1981.

Dietrich, W. E., R. Reiss, M.-L. Hsu, and D. R. Montgomery, A process-based model for colluvial soil depth and shallow landsliding using digital elevation data, *Hydrol. Processes*, *9*, 383–400, 1995.

Eagleson, P. S., *Dynamic Hydrology*, 462 pp., McGraw-Hill, New York, 1970.

Freeze, R. A., Streamflow generation, *Rev. Geophys*., *12*, 627–647, 1974.

Gillham, R. W., The capillary fringe and its effect upon water-table response, *J. Hydrol*., *67*, 307–324, 1984.

Green, W. H., and G. A. Ampt, Studies on soil physics, part I, The flow of air and water through soils, *J. Agric. Sci*., *4*, 1–24, 1911.

Haefeli, R., The stability of slopes acted upon by parallel seepage, *Proc. Int. Conf. Soil Mech. Found. Eng*., *1*, 57–62, 1948.

Haneberg, W. C., Observation and analysis of pore pressure fluctuations in a thin colluvium landslide complex near Cincinnati, Ohio, *Eng. Geol*., *31*, 159–184, 1991.

Hansen, A., Landslide hazard analysis, in *Slope Instability*, edited by D. Brunsden and D. B. Prior, pp. 523–604, John Wiley, New York, 1984.

Hurley, D. G., and G. Pantelis, Unsaturated and saturated flow through a thin porous layer on a hillslope, *Water Resour. Res*., *21*, 821–824, 1985.

Iverson, R. M., Unsteady, nonuniform landslide motion: Theory and measurement, Ph.D. dissertation, 303 pp., Stanford Univ., Stanford, Calif., 1984.

Iverson, R. M., Dynamics of slow landslides: A theory for time-dependent behavior, in *Hillslope Processes*, edited by A. D. Abrahams, pp. 297–317, Allen and Unwin, Winchester, Mass., 1986.

Iverson, R. M., Groundwater flow fields in infinite slopes, *Geotechnique*, *40*, 139–143, 1990.

Iverson, R. M., Sensitivity of stability analyses to groundwater data, in *Landslides* (*Proceedings of the Sixth International Symposium*), edited by D. H. Bell, pp. 451–457, Balkema, Rotterdam, Neth., 1991.

Iverson, R. M., The physics of debris flows, *Rev. Geophys*., *35*, 245–296, 1997.

Iverson, R. M., and J. J. Major, Rainfall, groundwater flow, and seasonal motion at Minor Creek landslide, northwestern California: Physical interpretation of empirical relations, *Geol. Soc. Am. Bull*., *99*, 579–594, 1987.

Iverson, R. M., M. E. Reid, and R. G. LaHusen, Debris flow mobilization from landslides, *Annu. Rev. Earth Planet. Sci*., *25*, 85–138, 1997.

Larsen, M. C., M. T. Vásquez Conde, and R. A. Clark, Landslide hazards associated with flash-floods, with examples from the December, 1999 disaster in Venezuela, in *Coping with Flash Floods*, edited by E. Gruntfest and J. Handmer, *NATO ASI Ser*., in press, 2000.

Leroueil, S., and M. E. S. Marques, Importance of strain rate and temperature effects in geotechnical engineering, in *Measuring and Modeling Time Dependent Soil Behavior*, edited by T. C. Sheahan and V. N. Kaliakin, pp. 1–60, Am. Soc. of Civ. Eng., New York, 1996.

Montgomery, D. R., and W. E. Dietrich, A physically based model for the topographic control on shallow landsliding, *Water Resour. Res*., *30*, 1153–1171, 1994.

Montgomery, D. R., W. E. Dietrich, R. Torres, S. P. Anderson, and J. T. Heffner, Hydrologic response of a steep unchanneled valley to natural and applied rainfall, *Water Resour. Res*., *33*, 91–109, 1997.

Reid, M. E., A pore-pressure diffusion model for estimating landslide-inducing rainfall, *J. Geol*., *102*, 709–717, 1994.

Reid, M. E., H. P. Nielson, and S. J. Dreiss, Hydrologic factors triggering a shallow hillslope failure, *Bull. Assoc. Eng. Geol*., *25*, 349–361, 1988.

Reid, M. E., R. G. LaHusen, and R. M. Iverson, Debris-flow initiation experiments using diverse hydrologic triggers, *Debris-Flow Hazards*

Mitigation: Mechanics, Prediction and Assessment, edited by C. L. Chen, pp. 1–10, Am. Soc. of Civ. Eng., New York, 1997.

Rib, H. T., and T. Lang, Recognition and Identification, in *Landslides Analysis and Control*, edited by R. L. Schuster and R. J. Krizek, *Transp. Res. Board Spec. Rep. 176*, pp. 34–80, Natl. Acad. of Sci., Washington, D. C., 1978.

Richards, L. A., Capillary conduction of liquids in porous mediums, *Physics*, *1*, 318–333, 1931.

Sidle, R. C., A theoretical model of the effects of timber harvesting on slope stability, *Water Resour. Res*., *28*, 1897–1910, 1992.

Smith, R. E., and R. H. B. Hebbert, Mathematical simulation of interdependent surface and subsurface hydrologic processes, *Water Resour. Res*., *19*, 987–1001, 1983.

Soeters, R., and C. J. van Westen, Slope instability recognition, analysis and zonation, in *Landslides: Investigation and Mitigation*, edited by A. K. Turner and R. L. Schuster, *Transp. Res. Board Spec. Rep. 247*, pp. 129–177, Natl. Acad. Press, Washington, D. C., 1996.

Swanson, F. J., and D. N. Swanston, Complex mass-movement terrains in the western Cascade Range, Oregon, *Rev. Eng. Geol*., *3*, 113–124, 1976.

Taylor, D. W., *Fundamentals of Soil Mechanics*, 700 pp., John Wiley, New York, 1948.

Terzaghi, K., *Erdbaumechanik*, Franz Deuticke, Vienna, 1925.

Terzaghi, K., Mechanism of landslides, in *Application of Geology to Engineering Practice* (*Berkey Volume*), edited by S. Paige, pp. 83–123, Geol. Soc. of Am., New York, Boulder, Colo., 1950.

Torres, R., W. E. Dietrich, D. R. Montgomery, S. P. Anderson, and K. Loague, Unsaturated zone processes and the hydrologic response of a steep, unchanneled catchment, *Water Resour. Res*., *34*, 1865–1879, 1998.

Van Genuchten, M. Th., A closed-form equation for predicting the hydraulic conductivity of unsaturated soils, *Soil Sci. Soc. Am. J*., *44*, 892–898, 1980.

Wieczorek, G. F., Effect of rainfall intensity and duration on debris flows in the central Santa Cruz Mountains, California, in *Debris Flows/Avalanches: Process, Recognition, and Mitigation*, edited by J. E. Costa and G. F. Wieczorek, pp. 93–104, Geol. Soc. of Am., Boulder, Colo., 1987.

Wu, W., and R. C. Sidle, A distributed slope stability model for steep forested basins, *Water Resour. Res*., *31*, 2097–2110, 1995.

R. M. Iverson, David A. Johnston Cascades Volcano Observatory, U.S. Geological Survey, 5400 MacArthur Boulevard, Vancouver, WA 98661. (riverson@usgs.gov)

(Received October 18, 1999; revised March 30, 2000; accepted March 30, 2000.)